# Characteristics of Gravity Waves in Opposing Phases of the QBO: A Reanalysis Perspective with ERA5

HAMID A. PAHLAVAN,[a,b] JOHN M. WALLACE,[a] QIANG FU,[a] AND M. JOAN ALEXANDER[b]

[a] *University of Washington, Seattle, Washington*
[b] *NorthWest Research Associates, Boulder, Colorado*

(Manuscript received 17 September 2023, in final form 24 May 2024, accepted 24 June 2024)

ABSTRACT: Gravity waves dispersing upward through the tropical stratosphere during opposing phases of the QBO are investigated using ERA5 data for 1979–2019. Log–log plots of two-sided zonal wavenumber–frequency spectra of vertical velocity, and cospectra representing the vertical flux of zonal momentum in the tropical lower stratosphere, exhibit distinctive gravity wave signatures across space and time scales ranging over two orders of magnitude. Spectra of the vertical flux of momentum are indicative of a strong dissipation of westward-propagating gravity waves during the easterly phase and vice versa. This selective "wind filtering" of the waves as they disperse upward imprints the vertical structure of the zonal flow on the resolved wave spectra, characteristic of (re)analysis and/or free-running models. The three-dimensional structures of the gravity waves are documented in composites of the vertical velocity field relative to grid-resolved tropospheric downwelling events at individual reference grid points along the equator. In the absence of a background zonal flow, the waves radiate outward and upward from their respective reference grid points in concentric rings. When a zonal flow is present, the rings are displaced downstream relative to the source and they are amplified upstream of the source and attenuated downstream of it, such that instead of rings, they assume the form of arcs. The log–log spectral representation of wind filtering of equatorial waves by the zonal flow in this paper can be used to diagnose the performance of high-resolution models designed to simulate the circulation of the tropical stratosphere.

KEYWORDS: Gravity waves; Inertia-gravity waves; Quasibiennial oscillation; Stratospheric circulation; Wave properties; Atmospheric waves

## 1. Introduction

Tropical convection excites gravity waves with a broad range of frequencies and horizontal scales that impact the global atmosphere by transporting energy and momentum over large horizontal and vertical distances and act as an important coupling mechanism between atmospheric layers (Fritts and Alexander 2003). The mechanism proposed by Lindzen and Holton (1968) to explain the downward propagation of easterly and westerly wind regimes in the QBO was based on the wind filtering of gravity waves with scales too small and frequencies too high to feel the effects of Earth's rotation. It is now well established that gravity waves do, in fact, contribute to the QBO wave forcing (e.g., Sato et al. 1994; Sato and Dunkerton 1997; Piani et al. 2000; Holt et al. 2020), particularly during the descent of the easterly shear zones (Giorgetta et al. 2002; Kawatani et al. 2010; Pahlavan et al. 2021a,b). The wind filtering of equatorially trapped planetary-scale waves also contributes to the descent of easterly and westerly wind regimes of the QBO, as noted in Lindzen and Holton (1968) and discussed in review articles by Baldwin et al. (2001) and Anstey et al. (2022). Determining the precise partitioning between various types of waves in the forcing of the QBO is still an active area of research. In particular, the limited resolution of the observations and the uncertainties in the representation of gravity waves in numerical models make it difficult to determine what fraction of the forcing is attributable to gravity waves.

In the companion paper (Pahlavan et al. 2023), we showed that the ERA5 reanalysis (Hersbach et al. 2020), with a horizontal resolution of 0.28° (~31 km), 137 hybrid model levels, and hourly temporal resolution, resolves a larger fraction of the gravity wave spectrum than its predecessors and thus provides valuable information on their behavior and spectral characteristics. In this paper, we extend the previous study by contrasting the properties of gravity waves in the tropical stratosphere during opposing phases of the QBO from 1979 to 2019, which spans approximately 16 QBO cycles. Leveraging a high-resolution, long-term simulation of gravity waves interacting with the QBO, constrained by the assimilation of extensive observational data, allows for a comprehensive analysis of gravity wave characteristics during opposing QBO phases.

Figure 1 provides an overview of the wind filtering that gives rise to the QBO, as represented in ERA5. It shows time–height sections of the vertical flux of zonal momentum over a 10-yr interval averaged over 10°S–10°N, superimposed upon the zonal wind field. QBO-related wave–mean flow interactions are clearly evident: Filtering of the wave spectrum by the mean flow systematically reduces the momentum flux by waves propagating in the same direction as the background flow. As a result, the net upward flux of zonal momentum is westward during the westerly phase of the QBO and eastward

Denotes content that is immediately available upon publication as open access.

*Corresponding author*: Hamid A. Pahlavan, pahlavan@nwra.com

DOI: 10.1175/JAS-D-23-0165.1

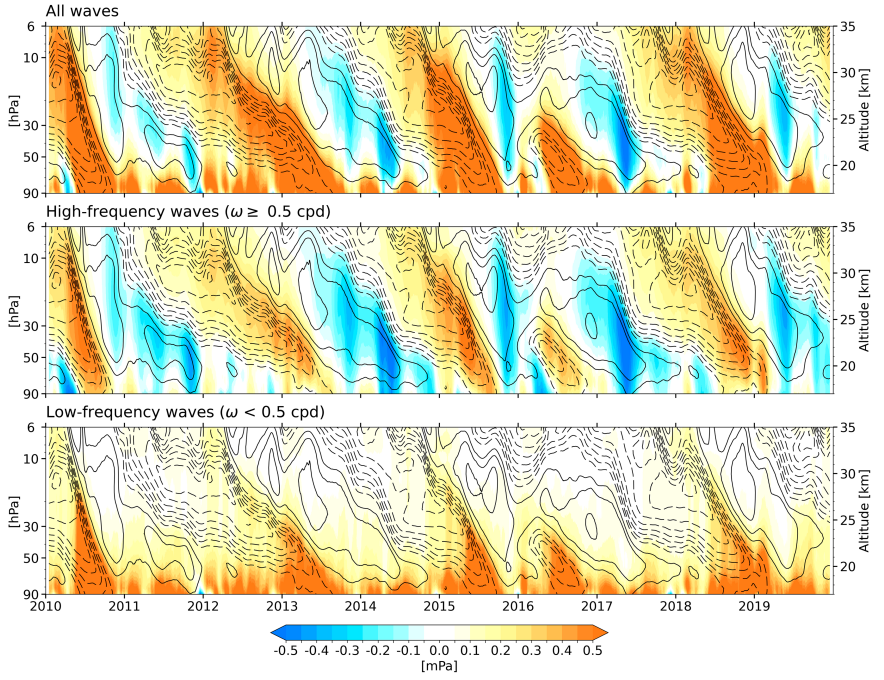


FIG. 1. Time–height sections of the vertical flux of zonal momentum (color shading) averaged over 10°S–10°N for (top) all waves, (middle) high-frequency waves (i.e., $\omega \geq 0.5$ cpd), and (bottom) low-frequency waves (i.e., $\omega < 0.5$ cpd), which is obtained as the difference between the top and middle panels. Contours indicate the zonally averaged zonal wind. The contour interval is 5 m $s^{-1}$, westerlies are solid, easterlies are dashed, and the zero contour is omitted. The results are based on hourly data, smoothed by a 30-day running mean. ERA5 model-level data are used in this figure.

during the easterly phase. The contribution of low-frequency waves, i.e., $\omega < 0.5$ cycles per day (cpd), to the total flux, shown in the bottom panel of Fig. 1, is dominated by the upward fluxes of eastward momentum associated with eastward-propagating Kelvin waves, which disperse upward with little dissipation until they encounter a westerly shear zone. They are largely confined to the lower stratosphere below the 30-hPa level. In contrast, the contribution from high-frequency waves (i.e., $\omega \geq 0.5$ cpd), shown in the middle panel, is dominated by inertio-gravity (IG) waves and gravity waves, which produce upward fluxes of eastward momentum in easterly wind regimes and upward fluxes of westward momentum in westerly wind regimes. The fluxes by the high-frequency waves extend through the depth of the stratosphere. The vertical flux of westward momentum by the IG and gravity waves is more intermittent, as reflected in the more irregular descent rate of the easterly shear zones. The purpose of this paper is to investigate the signature of wind filtering of waves by QBO-related perturbations of the zonal flow by contrasting wave-related spectra and composites observed in westerly and easterly regimes of the QBO.

Section 2 of this paper provides further specifics on the wind filtering based on two-sided zonal wavenumber–frequency spectra. To cover the wide range of space and time scales resolved by the ERA5 reanalysis, it is necessary to use logarithmic scales for wavenumber and frequency. Section 3 contrasts the structures of the gravity waves during opposing phases of the QBO based on compositing analysis. It is shown that the differences in spectra are consistent with the evolution of the three-dimensional structure of the waves as they disperse upward through background zonal wind profiles characteristic of westerly and easterly phases of the QBO. A brief discussion of the results and a few concluding remarks are presented in section 4.

The data and methods used in this study closely follow those in Pahlavan et al. (2023). The ERA5 data are hourly, retrieved at 0.25° × 0.25° horizontal resolution, and they span the period 1979–2019. We have used fields on both model levels and standard pressure levels.

## 2. Gravity wave spectra

To investigate the gravity wave spectra in opposing phases of the QBO, two-sided zonal wavenumber ($k$)–frequency ($\omega$) spectra and cospectra are calculated for dynamical variables on the latitude circles between 10°S and 10°N and averaged to obtain a single spectrum and cospectrum. As in Pahlavan et al. (2023), the spectra are plotted on logarithmic $k$ and $\omega$ scales and weighted by $k$ and $\omega$. Here, we examine the power spectrum of vertical velocity, which emphasizes the role of higher-frequency waves, and the cospectrum of vertical velocity and zonal wind, i.e., the vertical flux of zonal momentum, whose

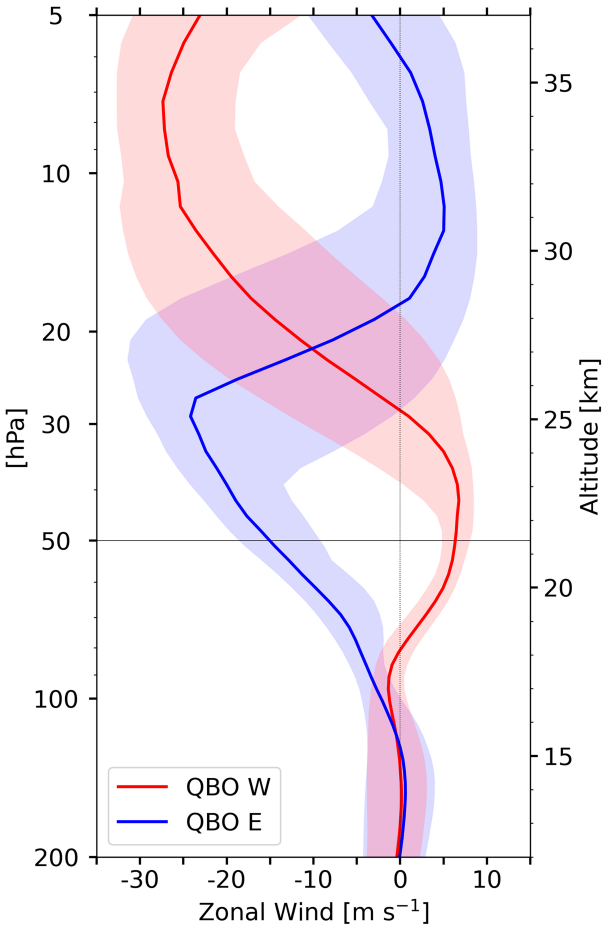


FIG. 2. Vertical profiles of zonally averaged zonal wind, averaged over 10°S–10°N based on the QBO phases at the 50-hPa level (marked by a horizontal gray line), for 1979–2019. The partitioning based on the 50-hPa level results in 228 months of the QBO W and 204 months of the QBO E. Solid lines indicate the median, and shadings indicate the quartiles (25% and 75%) of the monthly data. ERA5 model-level data are used in this figure.

vertical derivative is proportional to the zonal force exerted on the mean flow by resolved waves (exclusive of the Stokes drift in mixed Rossby–gravity waves).

The phase speed spectra of gravity waves with frequencies higher than 0.5 cpd are derived from the zonal wavenumber–frequency spectra. Each value in the $(k, \omega)$ domain is associated with a phase speed $c = \omega/k$. The phase speed spectrum is produced by grouping all the $(k, \omega)$ pairs into 2 m s$^{-1}$ phase speed bins and summing values in each phase speed bin. This binning procedure in the cospectrum yields the gravity wave contribution to the momentum flux as a function of ground-based zonal phase speed.

All calculations are averaged over specified time intervals corresponding to westerly or easterly phases of the QBO, which are defined based on the monthly mean zonal wind at the 50-hPa level. Values above 2 m s$^{-1}$ are assigned to the westerly phase (QBO W), and those below −2 m s$^{-1}$ are assigned to the easterly phase (QBO E). This partitioning yields 228 months of QBO W and 204 months of QBO E. Composite QBO W and QBO E zonal-mean zonal wind profiles are shown in Fig. 2.

First, let us consider the properties of power spectra of vertical velocity $w$ during opposing phases of the QBO. Figure 3 shows the two-sided zonal wavenumber–frequency power spectra at the 100-, 70-, and 50-hPa levels. The spectra are multiplied by density at each level, so that they represent the upward flux of upward momentum. Positive zonal wavenumbers correspond to eastward and negative values to westward-propagating waves. Lines of constant slope corresponding to the gravity waves with phase speeds of 23 and 49 m s$^{-1}$ are plotted for reference. See Pahlavan et al. (2023) for further discussion of these spectra and their characteristics and the slight preference for the two reference phase speeds, which are associated with the leading eigenmodes of convection in the tropical troposphere.

The 100-hPa spectrum is representative of waves dispersing upward from the troposphere into the stratosphere. The 70- and 50-hPa spectra illustrate the wind filtering of the waves as they disperse upward through the lower stratosphere. At the 100-hPa level, the $w$ spectra for QBO W and E are fairly similar, and as a result, the differences between them, shown in the bottom right panel, are quite small. In both QBO E and QBO W, the wave-related vertical velocity perturbations weaken with height from the 100- to 70-hPa levels, but upon close inspection (noting that the amplitude scale is logarithmic), it is evident that eastward-propagating waves experience somewhat greater damping during QBO W, while westward-propagating waves are more damped during QBO E. In the 70–50-hPa layer, the vertical velocity perturbations amplify slightly with height in the absence of critical layer absorption (i.e., for eastward-propagating waves in QBO E and westward-propagating waves in QBO W). Such wind filtering is responsible for the contrasting colors in the difference spectra for eastward- and westward-propagating waves in the top and middle panels of the right column of Fig. 3.

The differences between the QBO W and QBO E spectra vividly illustrate the workings of Lindzen and Holton's mechanistic model of the QBO, which is based on the principle that as a wave approaches its critical level, where its ground-based phase speed is equal to the background wind speed, its vertical wavelength and group velocity become small, and it becomes more susceptible to dissipation. Consequently, in QBO W, the eastward-propagating waves are preferentially weakened due to the presence of the westerly background flow and vice versa. The wave dissipation, in turn, forces the background flow, leading to the downward propagation of alternating westerly and easterly wind regimes.

Figure 4 shows phase speed spectra of $w$ for waves with frequencies $\omega \geq 0.5$ cpd in opposing phases of the QBO. At the 100-hPa level, the spectra for QBO E and QBO W are similar and nearly symmetric about the $y$ axis ($c = 0$ m s$^{-1}$), but they become increasingly asymmetric as the waves disperse upward: The eastward-propagating waves are strongly damped in QBO W and the westward-propagating waves are more strongly damped in QBO E. This wind-filtering signature is strongest for the waves with phase speeds $< 20$ m s$^{-1}$, but it

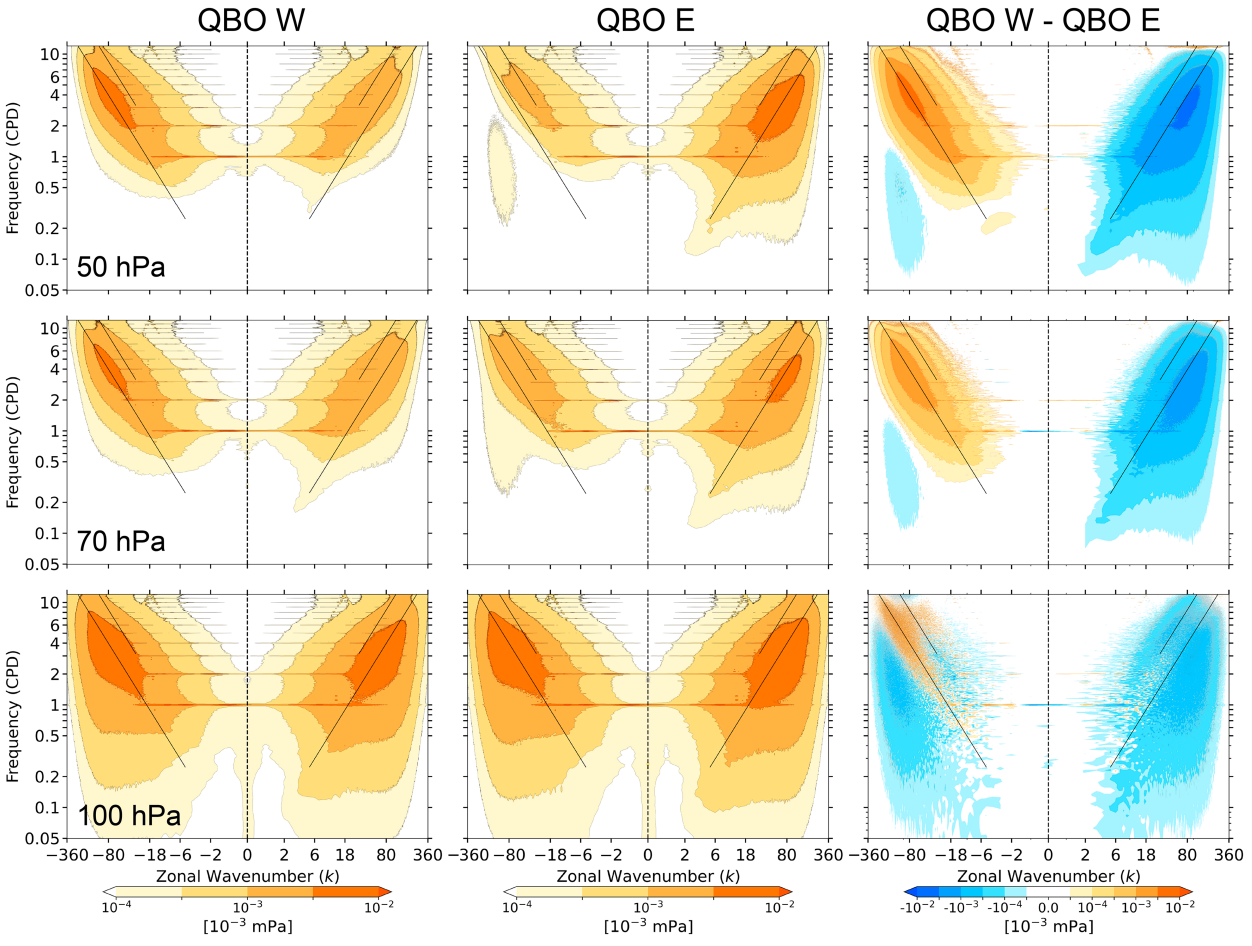


FIG. 3. Two-sided zonal wavenumber–frequency power spectra for the vertical velocity at the (top) 50-, (middle) 70-, and (bottom) 100-hPa levels, based on the QBO phases at the 50-hPa level. The spectra are shown on a logarithmic scale for wavenumber, frequency, and spectral density in unit of variance per unit area, from an average of the spectra computed at 1° latitude intervals between 10°S and 10°N based on hourly data. The spectral power is multiplied by $k \times \omega$ to preserve the property that (power × area) be proportional to variance anywhere on the plot. The contour interval corresponds roughly to a factor of 3. The sloping straight black lines correspond to phase speeds of $\pm 49$ m s$^{-1}$ (upper) and $\pm 23$ m s$^{-1}$ (lower). The scale of the zonal wavenumber is linear from $k = -1$ to 1.

is evident in waves with phase speeds as high as 60 m s$^{-1}$. The preferential wind filtering of more slowly propagating waves tends to flatten the spectra as the waves disperse upward.

Now, let us consider the spectra of vertical flux of zonal momentum $F_M$ in opposing phases of the QBO. The $F_M$ is the primary driver of the QBO, as shown in Figs. 8 and 9 of Pahlavan et al. (2021b), and its absolute value is a measure of the upward flux of wave activity. In the wavenumber–frequency spectra of $F_M$, shown in Fig. 5, positive values are indicative of an upward flux of eastward momentum, while negative values indicate an upward flux of westward momentum.

In contrast to the power spectrum of $w$ shown in Fig. 3, which is dominated by higher-frequency/smaller-scale gravity waves, the $F_M$ spectrum contains substantial contributions from Kelvin waves. The mixed Rossby–gravity (MRG) wave is also discernible as a patch of positive values centered ~0.25 cpd that extends across the zero wavenumber. Because of these features, the $F_M$ spectrum is not as symmetric about the $y$ axis ($k = 0$) as the $w$ spectrum.

As in the $w$ spectra in Fig. 3, the general decrease in $F_M$ in both the 100–70- and 70–50-hPa layers in both QBO E and QBO W is indicative of the existence of wave dissipation throughout the lower stratosphere. There is a stronger dissipation of eastward-propagating waves in QBO W and a stronger dissipation of westward-propagating waves in QBO E, as reflected in the dominance of blue shading in the difference spectra. Waves with phase speeds that fall within the range of zonal wind speeds in the QBO (−35 to +20 m s$^{-1}$) are much more strongly attenuated than waves with higher phase speeds. Hence, proceeding upward from the 100- to 50-hPa level, the peaks in the $F_M$ spectra are shifted toward higher phase speeds. At the 50-hPa level, the patch of positive values associated with the MRG wave is more prominent in QBO W than in QBO E, consistent with the notion of wind filtering.

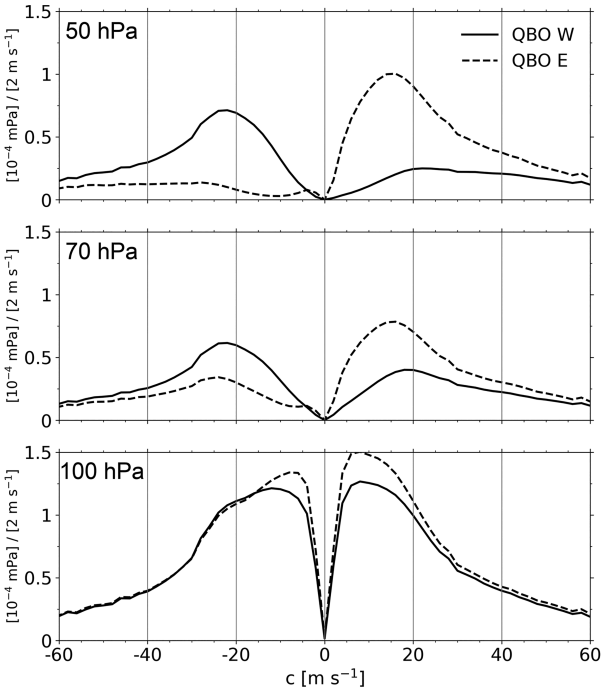


FIG. 4. Phase speed spectra of high-frequency waves (i.e., $\omega \geq 0.5$) obtained from vertical velocity power spectra at the (top) 50-, (middle) 70-, and (bottom) 100-hPa levels, based on the QBO phases at the 50-hPa level.

In contrast to the corresponding $w$ spectra, shown in Fig. 3, the swaths in the right panel of the $F_M$ cospectra shown in Fig. 5 exhibit sharp inner edges at a phase speed near the reference value of 23 m s$^{-1}$ for the eastward-propagating waves and slightly higher for the westward-propagating waves. This contrast shows the greater sensitivity of $F_M$ to the background zonal flow, attributable to the contribution of the zonal wind to $F_M$.

Figure 6 shows the phase speed spectra of $F_M$ for waves with frequencies $\omega \geq 0.5$ cpd. They are similar to the corresponding $w$ phase spectra, shown in Fig. 4, except that there is very little wind filtering for the westward-propagating waves faster than $-32$ m s$^{-1}$ and eastward-propagating waves faster than 23 m s$^{-1}$. As in the wavenumber–frequency spectra, the cutoff is quite abrupt.

The results from the two-sided spectra shown in Figs. 3 and 5 are summarized in Table 1, which is based on integrals over wavenumber and frequency ($\omega \geq 0.5$ cpd) of the spectra of the eastward- and westward-propagating waves observed in QBO E and QBO W. Wind filtering (i.e., weaker variances and covariances when the waves are dispersing upward through a layer in which the zonal wind and the propagation of the waves are in the same direction compared to when they are in opposing directions) is evident in both the 100–70- and 70–50-hPa layers and for both the variance of vertical velocity and covariance of the vertical flux of zonal momentum. The decline in the amplitude of the perturbations with height is much stronger in the 100–70-hPa layer than in the layer above. This is partially attributable to the greater depth of the 100–70-hPa layer (~30% thicker than the layer above, i.e., 2.4 vs 1.9 km). However, it is also possible that the variances and covariances at the 100-hPa level are not exclusively associated with gravity waves.

## 3. Gravity wave composites

In Pahlavan et al. (2023), we examined the three-dimensional structures of gravity waves by compositing different variables based on time series of tropospheric vertical velocity. In this subsection, we extend that analysis to investigate the structures of waves dispersing upward during opposing phases of the QBO.

The composites are based on the strongest downwelling events (i.e., those that fall in the top 10% of the frequency distribution) in a reference time series of tropospheric (the sum of 300 and 700 hPa) vertical velocity at individual grid points equally spaced along the equator at 1° intervals (i.e., 360 grid points). The composites for individual grid points are shifted in longitude so that they share a common reference grid point and then averaged together to form a single composite. The reference time series at each grid point closely resemble the leading principal component of the vertical profile of vertical velocity in the tropical troposphere and the heating profile in deep convection.

In the composites, QBO W and QBO E are defined based on the state of the zonal-mean zonal wind averaged over 10°S–10°N at the 20-hPa level. We chose a higher reference level for the compositing analysis than for the spectra because the zonal winds are stronger and the regimes are deeper when they are centered at 20 hPa than when they are centered at 50 hPa, and the distinctions between QBO E and QBO W are consequently clearer. Times when zonal wind is from the west and exceeds 2 m s$^{-1}$ are assigned to the QBO W composite and times when it is from the east and exceeds $-16$ m s$^{-1}$ are assigned to QBO E. This partitioning yields 156 months of QBO W and 227 months of QBO E. The corresponding composite QBO W and QBO E zonal-mean zonal wind profiles are shown in Fig. 7.

The top panels of Fig. 8 show composite horizontal maps of high-pass-filtered vertical velocity at the 10-hPa level in QBO W and E and the bottom panels show the corresponding equatorial longitude–height sections. The wind filtering of stratospheric waves results in departures from axial symmetry, leading to the downstream displacement of the centers of the rings. The waves upstream of the reference point are substantially stronger than those downstream of it. The asymmetries are more pronounced during QBO E (right panels) due to the greater strength (i.e., speed) of the easterly regimes. These results are consistent with previous observational and modeling studies (e.g., Piani et al. 2000; Yue et al. 2009; Vadas et al. 2012; Xu et al. 2015; Nyassor et al. 2021), which have reported that in the presence of weak background wind speeds, gravity waves propagate freely into the upper atmosphere so that their phase fronts are concentric circles, whereas when $|u| > 30$ m s$^{-1}$, they propagate mainly upstream and their phase fronts are elliptical, semielliptical, semicircular, or arc like.

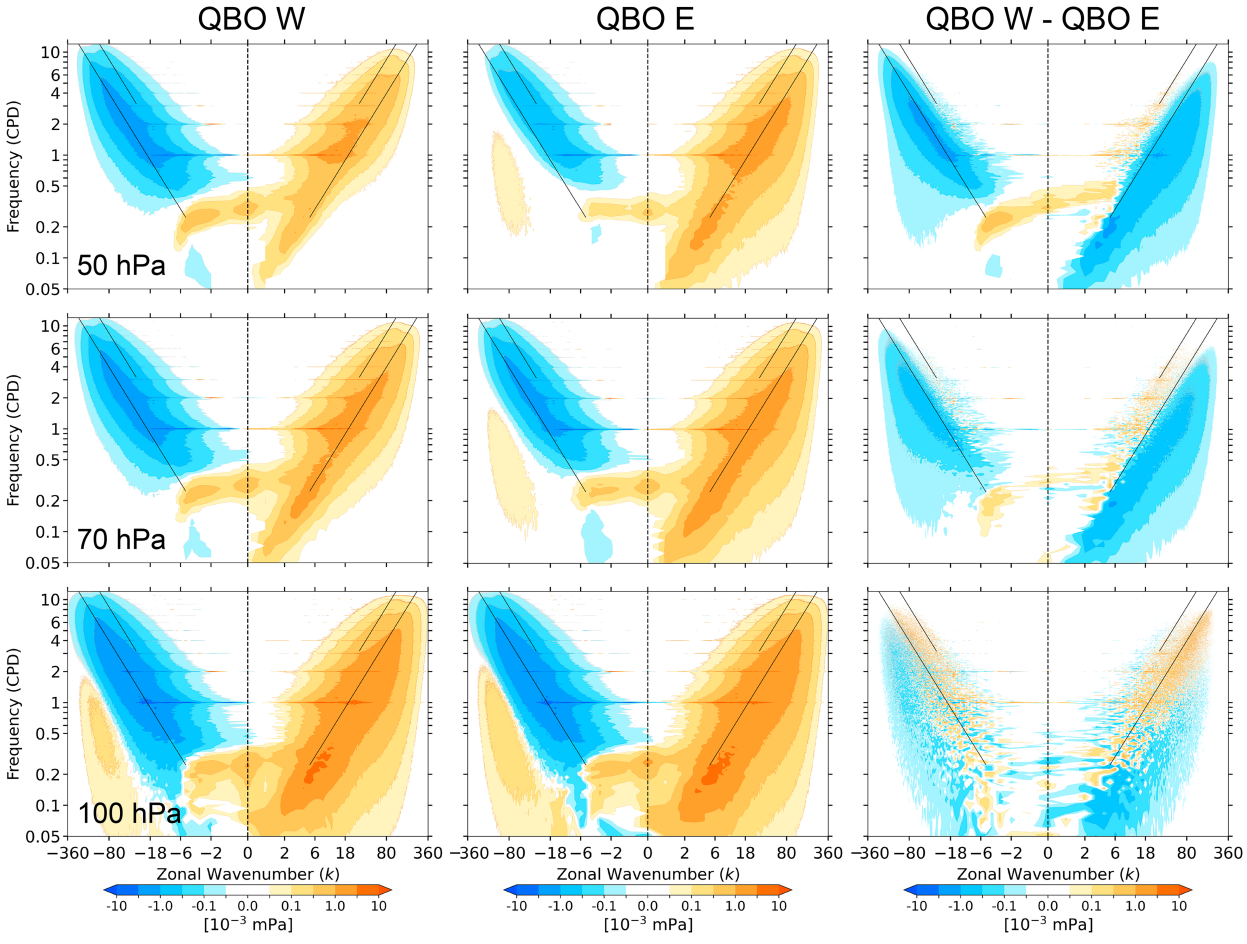


FIG. 5. As in Fig. 3, but for the vertical flux of zonal momentum $F_M$.

It also should be noted that these composites are based on the deep tropospheric mode, defined by the sum of standardized 700- and 300-hPa vertical velocities, for which the horizontal phase speed is ~50 m $s^{-1}$ (Pahlavan et al. 2023). Therefore, the waves can propagate through a westerly wind regime of the QBO, with $u \sim 15$ m $s^{-1}$ without being strongly dissipated, as can be seen in the left panels of Fig. 8.

## 4. Discussion and concluding remarks

Wind filtering of vertically propagating gravity waves by the zonally symmetric component of the flow is the essence of the mechanism proposed by Lindzen and Holton (1968) to explain the downward propagation of successive easterly and westerly wind regimes of the QBO.

Figure 5 provides a graphical perspective on wind filtering. The patterns are clearest at the 70-hPa level, where the waves have dispersed upward through a layer thinner than the typical depth of the easterly and westerly wind regimes of the QBO. The blue swaths in the difference spectrum, shown in the right panel, indicate the wavenumbers and frequencies that contribute most to the wind filtering. In the V-shaped zone in between them, the phase speeds of the waves are sufficiently high that the waves in both QBO E and QBO W are able to disperse upward without being strongly dissipated. That the strong wind filtering extends to slightly higher frequencies for the westward-propagating waves than for the eastward-propagating waves reflects the higher zonal wind speeds in QBO E. The edge of the filtering-free zone shifts slightly toward higher phase speeds from the 70- to 50-hPa level, perhaps because of the higher amplitude of the QBO E and QBO W regimes at the higher level. There is no trace of the wind-filtering signature at the 100-hPa level.

The study of Lindzen and Holton (1968) was motivated, in part, by the discovery of equatorially trapped, vertically propagating planetary waves—i.e., MRG waves (Yanai and Maruyama 1966) and Kelvin waves (Wallace and Kousky 1968). In the interests of simplicity, they framed their mechanistic model of the QBO in terms of zonally propagating gravity waves, but one of their recommendations for future research was that "the interaction between gravity waves and the mean flow should be explicitly studied for gravity waves modified by the Earth's rotation."

The schematic shown in Fig. 9 provides a comprehensive summary of the roles of Kelvin, MRG, IG, and gravity waves in forcing the descent of westerly and easterly wind regimes of the QBO. In prescribing the equivalent depth in the

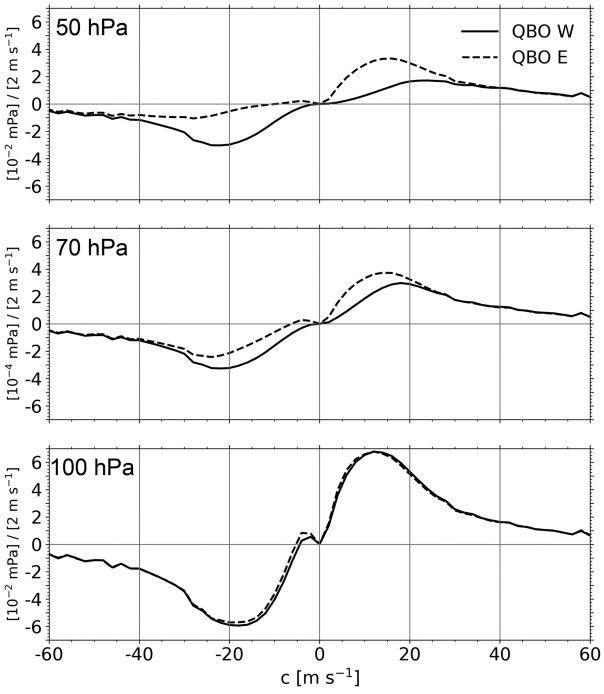


FIG. 6. As in Fig. 4, but for the vertical flux of zonal momentum.

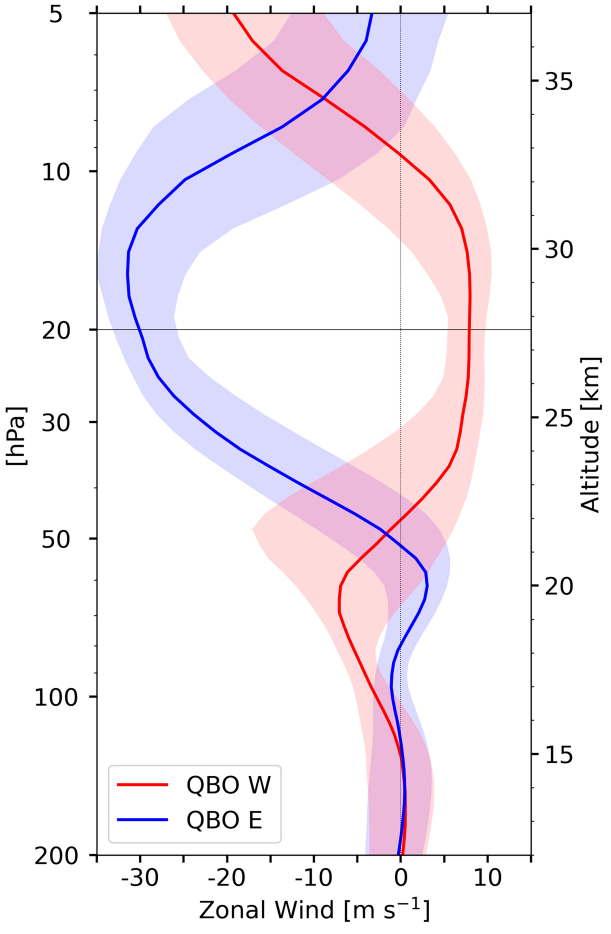


FIG. 7. As in Fig. 2, but based on the QBO phases at the 20-hPa level.

dispersion diagram, we use the observed phase speed of the stratospheric Kelvin wave (32 m $s^{-1}$). In the dispersion diagram for equatorially trapped waves, eastward-propagating waves with frequencies lower than that of the MRG wave are exclusively Kelvin waves: those with frequencies higher than that are a mix of Kelvin, IG, and gravity waves. Westward-propagating waves with frequencies higher than that of the MRG wave are exclusively IG and gravity waves and those with lower frequencies are MRG waves. The signature of the MRG wave is clearly apparent in Fig. 9 as a "bridge" of positive values crossing the $y$ axis ($k = 0$) at frequencies close to 0.25 cpd. Bearing in mind that eastward-propagating waves are responsible for the descent of westerly wind regimes of the QBO and westward-propagating waves for the descent of easterly wind regimes, the contribution of Kelvin waves to the descent of westerly regimes and IG and gravity waves to the descent of both easterly and westerly regimes is abundantly clear.

The contribution of MRG waves to the descent of easterly regimes, which is mediated by the Stokes drift induced by the poleward eddy heat fluxes by the waves, is not represented in Fig. 9. In Pahlavan et al. (2021b), we calculated the contribution of the MRG-related forcing to the descent of easterly wind regimes using the transformed Eulerian mean formulation of the zonal momentum equation and found it to be slightly smaller than the IG wave contribution. Just how much the gravity waves contribute to the wind filtering is dependent upon the model resolution.

In discussing the spectra presented in section 2, we have considered only the evidence related to wind filtering. At the 100-hPa level, there is little or no QBO-related wind filtering of gravity waves because, at that level, the zonal winds in QBO E and QBO W differ by only a few meters per second (Fig. 2). Yet it is evident from the bottom right panel of Fig. 3 that the amplitude of both eastward- and westward-propagating waves is stronger in QBO E, except for a narrow band with phase speeds around −23 m $s^{-1}$. It is conceivable that these differences are thermodynamically induced. The tropical cold point tropopause is not quite as cold in QBO W as in QBO E. A colder tropopause is conducive to deeper convection (Sweeney et al. 2023), which could serve as a stronger source of gravity waves. It may not

TABLE 1. The ratio of the variance of vertical velocity and the covariance of the vertical flux of zonal momentum (in parentheses), between the vertical levels, based on integrals over wavenumber and frequency ($\omega \geq 0.5$ cpd) of the spectra presented in Figs. 3 and 5.

| | QBO W | | QBO E | |
|---|---|---|---|---|
| Levels (hPa) | Westward | Eastward | Westward | Eastward |
| 50/70 | 1.12 (0.93) | 0.83 (0.73) | 0.67 (0.57) | 1.22 (0.92) |
| 70/100 | 0.52 (0.6) | 0.42 (0.52) | 0.36 (0.47) | 0.58 (0.62) |

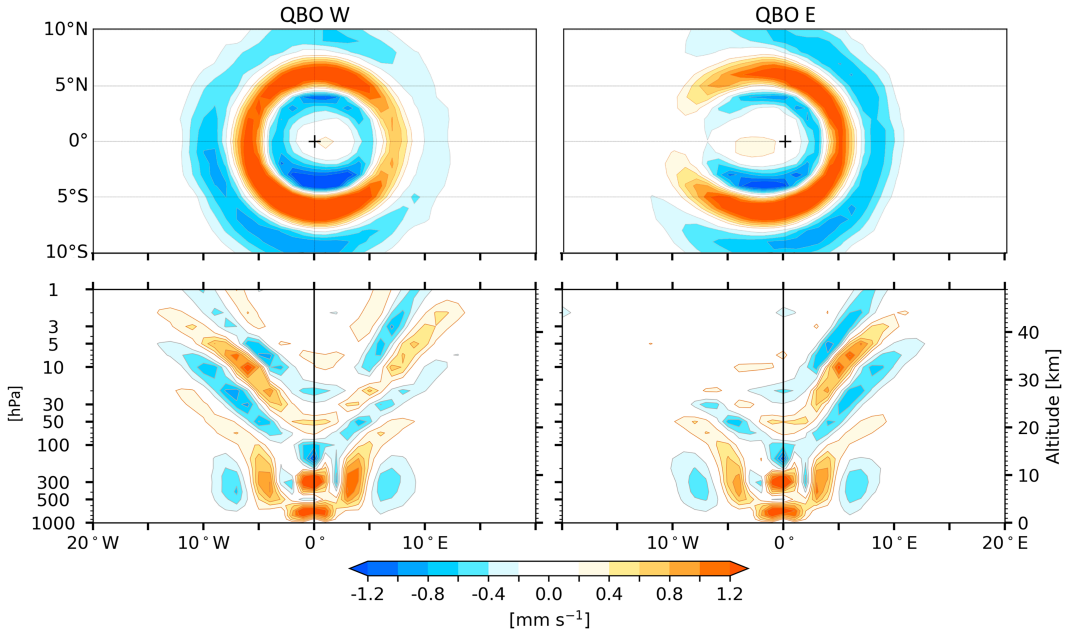


FIG. 8. Composites of high-pass-filtered vertical velocity constructed based on the top 10% of strongest downwelling events at individual reference grid points along the equator, shown 8 h after the events, using hourly data for 1979–2019, and based on the QBO phases at the 20-hPa level. The reference time series is the sum of the standardized 700- and 300-hPa vertical velocity (see Pahlavan et al. 2023 for more detail). (top) Horizontal cross sections of vertical velocity at the 10-hPa level. (bottom) The corresponding longitude–height cross sections along the equator. The reference grid point is shown by a cross in the top panels.

be entirely coincidental that waves with phase speeds of ~23 m s$^{-1}$ behave differently from other waves (see also Fig. 5). This phase speed matches that of the second mode of tropospheric convection, which involves fluctuations between top-heavy and bottom-heavy deep convection in the tropics (Takayabu et al. 1996). A more detailed analysis of the impact of the QBO at the 100-hPa level and below is left for future study.

The spectral representation of the variances and covariances employed in this paper based on two-sided spectra plotted on a logarithmic scale should be useful for evaluating and comparing the performance of the various reanalyses and free-running atmospheric models used to simulate the QBO.

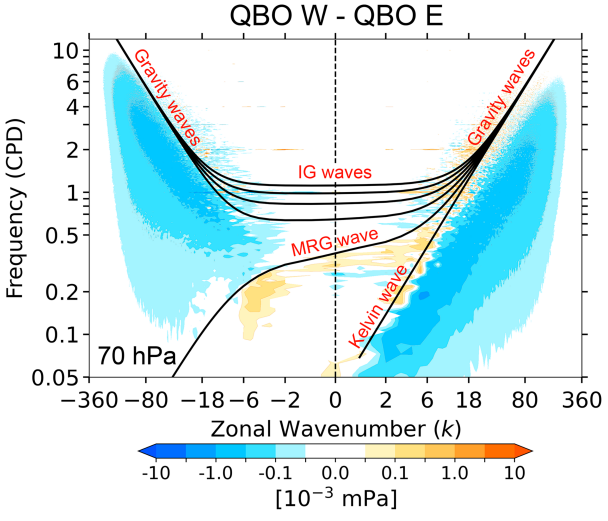


FIG. 9. As in the middle panel in the right column of Fig. 5, but with theoretical dispersion curves for a system of dry shallow-water equations on an equatorial beta plane, with an equivalent depth of 104 m to match the observed phase speed of the stratospheric Kelvin wave (32 m s$^{-1}$).

*Acknowledgments.* This research is supported by the NSF Grant AGS-2202812. The authors declare no conflicts of interest.

*Data availability statement.* ERA5 model-level data used in Figs. 1, 2, and 7 were downloaded from ECMWF's MARS archive, while pressure-level data used in the remaining figures were downloaded from the Copernicus Climate Data Store (https://cds.climate.copernicus.eu/).

## REFERENCES

Anstey, J. A., and Coauthors, 2022: Impacts, processes and projections of the quasi-biennial oscillation. *Nat. Rev. Earth Environ.*, **3**, 588–603, https://doi.org/10.1038/s43017-022-00323-7.

Baldwin, M. P., and Coauthors, 2001: The quasi-biennial oscillation. *Rev. Geophys.*, **39**, 179–229, https://doi.org/10.1029/1999RG000073.

Fritts, D. C., and M. J. Alexander, 2003: Gravity wave dynamics and effects in the middle atmosphere. *Rev. Geophys.*, **41**, 1003, https://doi.org/10.1029/2001RG000106.

Giorgetta, M. A., E. Manzini, and E. Roeckner, 2002: Forcing of the quasi-biennial oscillation from a broad spectrum of atmospheric waves. *Geophys. Res. Lett.*, **29**, 1245, https://doi.org/10.1029/2002GL014756.

Hersbach, H., and Coauthors, 2020: The ERA5 global reanalysis. *Quart. J. Roy. Meteor. Soc.*, **146**, 1999–2049, https://doi.org/10.1002/qj.3803.

Holt, L. A., and Coauthors, 2020: An evaluation of tropical waves and wave forcing of the QBO in the QBOi models. *Quart. J. Roy. Meteor. Soc.*, **148**, 1541–1567, https://doi.org/10.1002/qj.3827.

Kawatani, Y., S. Watanabe, K. Sato, T. J. Dunkerton, S. Miyahara, and M. Takahashi, 2010: The roles of equatorial trapped waves and internal inertia–gravity waves in driving the quasi-biennial oscillation. Part I: Zonal mean wave forcing. *J. Atmos. Sci.*, **67**, 963–980, https://doi.org/10.1175/2009JAS3222.1.

Lindzen, R. S., and J. R. Holton, 1968: A theory of the quasi-biennial oscillation. *J. Atmos. Sci.*, **25**, 1095–1107, https://doi.org/10.1175/1520-0469(1968)025<1095:ATOTQB>2.0.CO;2.

Nyassor, P. K., and Coauthors, 2021: Case studies on concentric gravity waves source using lightning flash rate, brightness temperature and backward ray tracing at São Martinho da Serra (29.44°S, 53.82°W). *J. Geophys. Res. Atmos.*, **126**, e2020JD034527, https://doi.org/10.1029/2020JD034527.

Pahlavan, H. A., Q. Fu, J. M. Wallace, and G. N. Kiladis, 2021a: Revisiting the quasi-biennial oscillation as seen in ERA5. Part I: Description and momentum budget. *J. Atmos. Sci.*, **78**, 673–691, https://doi.org/10.1175/JAS-D-20-0248.1.

——, J. M. Wallace, Q. Fu, and G. N. Kiladis, 2021b: Revisiting the quasi-biennial oscillation as seen in ERA5. Part II: Evaluation of waves and wave forcing. *J. Atmos. Sci.*, **78**, 693–707, https://doi.org/10.1175/JAS-D-20-0249.1.

——, ——, and ——, 2023: Characteristics of tropical convective gravity waves resolved by ERA5 reanalysis. *J. Atmos. Sci.*, **80**, 777–795, https://doi.org/10.1175/JAS-D-22-0057.1.

Piani, C., D. Durran, M. J. Alexander, and J. R. Holton, 2000: A numerical study of three-dimensional gravity waves triggered by deep tropical convection and their role in the dynamics of the QBO. *J. Atmos. Sci.*, **57**, 3689–3702, https://doi.org/10.1175/1520-0469(2000)057<3689:ANSOTD>2.0.CO;2.

Sato, K., and T. J. Dunkerton, 1997: Estimates of momentum flux associated with equatorial Kelvin and gravity waves. *J. Geophys. Res.*, **102**, 26 247–26 261, https://doi.org/10.1029/96JD02514.

——, F. Hasegawa, and I. Hirota, 1994: Short-period disturbances in the equatorial lower stratosphere. *J. Meteor. Soc. Japan*, **72**, 859–872, https://doi.org/10.2151/jmsj1965.72.6_859.

Sweeney, A., Q. Fu, H. A. Pahlavan, and P. Haynes, 2023: Seasonality of the QBO impact on equatorial clouds. *J. Geophys. Res. Atmos.*, **128**, e2022JD037737, https://doi.org/10.1029/2022JD037737.

Takayabu, Y. N., K.-M. Lau, and C.-H. Sui, 1996: Observation of a quasi-2-day wave during TOGA COARE. *Mon. Wea. Rev.*, **124**, 1892–1913, https://doi.org/10.1175/1520-0493(1996)124<1892:OOAQDW>2.0.CO;2.

Vadas, S., J. Yue, and T. Nakamura, 2012: Mesospheric concentric gravity waves generated by multiple convective storms over the North American Great Plain. *J. Geophys. Res.*, **117**, D07113, https://doi.org/10.1029/2011JD017025.

Wallace, J. M., and V. E. Kousky, 1968: Observational evidence of Kelvin waves in the tropical stratosphere. *J. Atmos. Sci.*, **25**, 900–907, https://doi.org/10.1175/1520-0469(1968)025<0900:OEOKWI>2.0.CO;2.

Xu, J., and Coauthors, 2015: Concentric gravity waves over northern China observed by an airglow imager network and satellites. *J. Geophys. Res. Atmos.*, **120**, 11 058–11 078, https://doi.org/10.1002/2015JD023786.

Yanai, M., and T. Maruyama, 1966: Stratospheric wave disturbances propagating over the equatorial Pacific. *J. Meteor. Soc. Japan*, **44**, 291–294, https://doi.org/10.2151/jmsj1965.44.5_291.

Yue, J., and Coauthors, 2009: Concentric gravity waves in the mesosphere generated by deep convective plumes in the lower atmosphere near Fort Collins, Colorado. *J. Geophys. Res.*, **114**, D06104, https://doi.org/10.1029/2008JD011244.